Contents lists available at ScienceDirect

Applied Catalysis A, General

Highly dispersed copper oxide on silica: Towards an efficient catalyst for continuous glycerol dehydration to acetol

Jaime Mazarío [a], Juan A. Cecilia [b], Enrique Rodríguez-Castellón [b], Marcelo E. Domine [a],[*]

[a] *Instituto de Tecnología Química (UPV-CSIC), Universitat Politècnica de València, Consejo Superior de Investigaciones Científicas, Avda. Los Naranjos S/N, 46022 Valencia, Spain*
[b] *Departamento de Química Inorgánica, Cristalografía y Mineralogía (Unidad Asociada al ICP-CSIC), Facultad de Ciencias, Universidad de Málaga, Campus de Teatinos, 29071 Málaga, Spain*

ARTICLE INFO

ABSTRACT

In most current processes aimed at producing biodiesel glycerol is still a co-product, and its valorisation is essential for the biorefinery. This work relies on previous results showing the dependence of the selective dehydration of glycerol to acetol (hydroxyacetone) on achieving a moderate acidity and the redox functionality of copper to complete the chemical process. In this sense, this reaction was studied using CuO supported on silica. Different silicas and copper incorporation methodologies were investigated to develop the best CuO/SiO$_2$ material. Interestingly, these CuO-based materials developed acidity and became more active when increasing the copper oxide dispersion, thereby going from poorly to intensely effective to dehydrate glycerol selectively to acetol. Catalysts were characterised by different techniques (i.e., ICP, N$_2$ adsorption, XRD, TPR, HR-TEM, etc.) to explain the differences observed in catalytic activity and acetol yield based on their physicochemical properties.

1. Introduction

Over the last decades, a wide array of so-called biofuels (i.e., bio-ethanol, biodiesel, biogas) have emerged in the market in an effort to diminish the worldwide dependence on fossil sources [1,2]. With respect to biodiesel, it is produced by transesterification of triglycerides (vegetable oils) with methanol or ethanol to yield methyl or ethyl-esters [3–5]. However, in correspondence with the food industry constraints on the use of agricultural land, the trend nowadays is towards biodiesel production from unconventional raw materials (i.e., cooking oils, animal fats, agricultural and domestic wastes, etc.) [6,7]. Nonetheless, even in these novel instances, vast amounts of glycerol are also formed as a co-product, whose valorisation is still a significant challenge if the biorefinery wants the process to be profitable. Thus, there has been an academic struggle by many research groups working in catalysis, which have broadly studied glycerol transformation and valorisation [8–11].

Many possibilities of valorisation for this molecule spanning heterogeneous catalysis have been established in the last years. Selective oxidation to yield valuable oxygenated derivatives (dihydroxyacetone, glyceric acid, hydroxypyruvic acid, mesooxalic acid, tartronic acid, lactic acid) [12,13], hydrogenolysis to propanediols [14], or ethylene glycol [15], catalytic dehydration to either acrolein or hydroxyacetone [16], synthesis of glycerol carbonate [17], oligomerization and polymerisation [18], acetalization and ketalization [19,20] or transesterification to monoglycerides [21] are just amongst the many examples that can be found in the recent literature.

Particularly, the selective dehydration of glycerol to acetol (hydroxyacetone) is of interest considering the reactivity of this molecule, having a terminal hydroxyl group and a carbonyl group in the second carbon. These functional features give acetol the possibility of taking part in different organic reactions, such as the Mannich reaction or some aldolic condensations [22,23]. More recently, our group illustrated how acetol could be used as a carbon source to produce nitrogenated heterocycles [24]. Besides that, acetol is a crucial intermediate when synthesising other high added-value compounds from glycerol, such as propylene glycol [25].

As far as the production of acetol is concerned, not so many studies have been recounted. The highest yield of acetol from glycerol was obtained in a reactive distillation system with copper chromite as catalyst (≈80% yield) [26], being the main shortcomings of the process, the catalyst toxicity, and the difficulty to be scaled-up. At present, a scarce group of heterogeneous catalysts Cu-Al$_2$O$_3$ [27], La$_2$CuO$_4$ [28], Cu-MgAlO$_x$ [29], and Cu-MgF$_2$ [30] are the only ones capable of carrying out the reaction effectively in a continuous system and in the absence of

---

hydrogen. Nevertheless, common drawbacks such as moderate yields, deactivation by coke deposition, and copper sintering are still problematic. Additionally, for the La$_2$CuO$_4$ catalyst, an additional disadvantage is the need for vaporising glycerol at $\geq$ 300 ºC before feeding it into the reactor.

Owing to the substantial number of studies to produce the other glycerol dehydration product, acrolein, Brönsted acid sites are well known to present higher selectivity to acrolein. On the contrary, Lewis acid sites could offer a superior selectivity towards acetol [16]. Additionally, the constant presence of Cu in the so-far reported catalysts is the cause of a sharp increase in activity and acetol selectivity at temperatures where, else wise, the same material but without Cu would be practically inactive. Nonetheless, the reaction mechanism is still under debate and, until recent times, convincing explanations of the role of copper were conspicuously absent. Sato et al. ascribed this effect to the inherent ability of Cu to cleave the C–O bond preferentially to the C–C bond in glycerol hydrogenolysis [27]. Another suggested possibility is that the reaction occurring over Cu sites should consist of a dehydrogenation-dehydration-(re)hydrogenation sequence [31,32]. However, little "in-situ" characterisation has been provided to determine which is the evolution of the Cu oxidation state throughout the process and, hence, the essential nature of the Cu active site for this reaction.

Following this idea, our previous research work focussed on developing Cu-based mixed oxides and understanding the role of every active centre involved in the reaction, i.e., Lewis acids, Lewis bases, and copper (redox properties). By means of different "in-situ" spectroscopies (XPS, FTIR), we proved that the copper reducibility and, more specifically, the presence of Cu^{1+} species during the reaction is crucial to carry out the first step of the reaction, involving a glyceraldehyde formation [29]. The higher reactivity of this Cu^{1+} species had recently been suggested by catalytic and DFT studies [30].

Moreover, we reported that moderate Lewis acidity seems to be required to allow the glycerol first adsorption on the catalyst [29]. This conclusion has recently been supported by R.J. Chimentão et al., showing by DFT and backed by catalytic results the critical role of acid sites of supports to promote glycerol interaction [33]. Nevertheless, an overabundance of acidity results in undesired by-products, higher carbon deposits and a pronounced catalyst deactivation [34,35]. Therefore, aiming at carefully tuning the acidity of the materials, the selection of copper support/matrix is essential to optimise the process.

In this sense, several years ago, N. Ravasio and co-workers reported that unexpected Lewis acidity could arise on CuO/SiO$_2$ depending on the level of Cu-dispersion obtained with the preparation technique employed [36,37]. According to them, the surface defectivity of dispersed CuO, would result in coordinative unsaturation of Cu atoms, making them more susceptible to coordinate molecules from the surroundings. The plausible reasons behind this surge in acidity with an increased dispersion are still under debate, though, with other authors finding solid correlations indicating that, in highly dispersed CuO/SiO$_2$ materials, the Cu-O-Si sites should be held accountable for the greater strength in the material acidity [38].

This novel relationship between dispersion and acidity could dictate a new basis for their use in a broad range of applications, keeping other commonly known properties of Cu such as hydrogenation and dehydrogenation activity. This is especially interesting for our reaction, given that CuO-SiO$_2$ systems have frequently been reported as materials that can be highly selective to acetol [27,34]. However, they lack the essential acidity to carry out the reaction with high glycerol conversions compared to other systems such as CuO-Al$_2$O$_3$ [33]. Therefore, the aim of this work is finding a suitable acidity to boost catalyst activity without impairing selectivity on the CuO-SiO$_2$ system. Doing it through enhancing metal dispersion seems a novel and exciting approach to improve the catalytic behaviour of the CuO-SiO$_2$ system in this alternative for glycerol valorisation that is its dehydration to acetol.

In this regard, highly dispersed copper oxide on silica is herein prepared and reported as a highly efficient catalyst to carry out glycerol dehydration to acetol. As a result of its moderate acidity, the CuO/SiO$_2$ material here prepared exhibits comparable or even superior activity and lower tendency to side reactions than other already reported catalysts. Thereafter, introduction of mesoporosity in the best material was attempted to improve even more dispersion and/or stability of Cu species.

2. Experimental

2.1. Catalyst preparation

Different catalysts were prepared by supporting a Cu precursor on SiO$_2$ from Chempur (SiO$_2$-CH, $\approx$250 m^2/g, see Table S1) and SiO$_2$ fumed from Sigma-Aldrich (SiO$_2$-AL, $\approx$350 m^2/g, see Table S1). Such incorporation was carried out, for the SiO$_2$-CH, by the incipient wetness impregnation (IW) method (CuO-IW/SiO$_2$-CH), using an aqueous solution of Cu(NO$_3$)$\cdot$2.5H$_2$O with the adequate concentration to achieve a 5 wt% Cu in the final solid. After the addition, the slurry was dried at 100 ºC overnight.

For the two commercial SiO$_2$, the precipitation-deposition method (PD) with urea (Sigma-Aldrich, 99.0–100.0 wt%) as the precipitant agent (CuO-PD/SiO$_2$-CH and CuO-PD/SiO$_2$-IW) was also used. Typically, 2 g of silica were dispersed in 100 mL of deionized water, 2.7 g of urea and the appropriate amount of Cu(NO$_3$)$\cdot$3H$_2$O to get Cu loadings of around 5 wt%. This mixture was stirred at 90 ºC for two hours. After this time, the solid was filtered and dried overnight at 80 ºC.

Also, for the SiO$_2$-AL, functionalization of the silica with aminopropyl groups (AP) was carried out before incorporating the Cu precursor (CuO-AP/SiO$_2$-AL). 2 g of porous silica were dried overnight under a He flow, at 115 ºC, and added to a solution of 3 aminopropyltriethoxysilane (APTES), by using dry toluene (15 mL) as the solvent, under reflux at 110 ºC for 24 h. After the grafting, the solid was filtered, washed with toluene, and dried overnight at 120 ºC. In the next step, the SiO$_2$-AL was stirred with an aqueous solution of Cu (NO$_3$)$_2\cdot$3H$_2$O in 100 mL of deionized water (5 Cu wt% to the porous silica) and 2.7 g of urea for 2 h. Finally, the solid was filtered and dried overnight at 80 ºC.

After the drying step, all the solids underwent a calcination treatment in air; at 550 ºC (6 h) for those materials prepared by IW and at 400 ºC (2 h) for materials prepared by PD and AP. For comparative purposes, 5 wt% Cu was also added by wetness impregnation on γ-Al$_2$O$_3$ (Al$_2$O$_3$ Nanopowder, Sigma-Aldrich).

In addition, SBA-15 type mesoporous silica was prepared following the methodology described by Fulvio et al. [39]. Thus, Pluronic P-123 was dissolved in a solution of HCl (1.7 M, Sigma-Aldrich) at 40 ºC. Subsequently, tetraethyl orthosilicate (TEOS, 98%, Sigma-Aldrich) was added dropwise to the Pluronic solution. After incorporating the Si source, the gel was transferred to a 90 mL Teflon-lined autoclave, for a hydrothermal treatment at 80 ºC for 48 h. This material was also used to support the CuO moieties by using the precipitation-deposition method (PD).

2.2. Catalyst characterisation

Cu content was determined by ICP (inductively coupled plasma) with a Varian 715-ES ICP-Optical Emission spectrometer after dissolution in HNO$_3$/HCl/HF aqueous solution (1:1:1 vol). The instrument was previously calibrated for Cu measurement. Phase purity of all the SiO$_2$-based catalysts was determined by X-ray diffraction (XRD) in a Philips X'Pert MPD diffractometer equipped with a PW3050 goniometer (CuKα radiation), at a scan rate of 2 min^{-1}, operating at 40 kV and 35 mA, provided with a variable divergence slit and working in the fixed irradiated area mode. For the SBA-15 type material, data was collected stepwise over the $0.71° \leq 2\theta \leq 7.00°$ angular region, with steps of 0.02° 2θ, 20 s/step accumulation time. Experimental diffractograms were

compared with those found at the PDF2 database (codes in parenthesis). High-resolution electronic transmission microscopy (HR-TEM) study of fresh and used catalysts was performed in Jeol JEM-2100 F equipment, working at 200 kV. HR micrograph analysis, lattice spacing measurement, first Fourier transform (FFT), and phase interpretation were made using the Gatan Digital Micrograph software (Gatan Inc.) and the Java version of the electron microscope software (JEM). X-ray photoelectron spectra (XPS) were collected on a SPECS spectrometer equipped with Phoibos 150MCD-9 analyser and using a non-monochromatic Al Kα (1486.6 eV) X-ray source. Spectra were recorded at 25 °C, using an analyser pass energy of 30 eV, an X-ray power of 50 W, and under an operating pressure of 10^{-9} mbar. A 20 mins acquisition time was never surpassed to avoid photo-reduction of Cu. Intensities were corrected by the transmission function of the spectrometer. Spectra treatment was performed using the CASA software. Gaussian–Lorentzian curves and nonlinear-Shirley background subtraction were used for peak fitting. During data processing of the XPS spectra, binding energy (BE) values were referenced to the Si_{2p} peak at 103.4 eV [40,41].

Surface areas of the solid samples (200 mg) were calculated using liquid nitrogen adsorption experiments at − 196 °C, in a Micromeritics flowsorb apparatus. The BET surface area was determined applying the theory of Brunauer, Emmett, and Teller but fulfilling the criterion established by Rouquerol et al. [42], according to which the relative pressure range for BET surface area determination was limited to the range $P/P^0 = 0.05$–0.25 of the N_2 adsorption isotherms. For the SBA-15 type material, the pore diameter and the pore size distribution were calculated using the Barret−Joyner−Halenda (BJH) method on the N_2 adsorption branch of the isotherms. Acid centres present in our materials were determined by temperature-programmed desorption of ammonia (NH_3-TPD) carried out on a TPD/2900 apparatus from Micromeritics. Nearly 0.100 g of sample were pre-treated in an Ar stream at 300 °C for 1 h. Ammonia was chemisorbed by pulses at 100 °C until equilibrium was reached. The sample was then fluxed with a He stream for 15 min before increasing the temperature up to 500 °C in a He stream of 100 mL/min and using a heating rate of 10 °C/min. Gas adsorption was monitored with a calibrated thermal conductivity detector (TCD), representing a quantitative value. Besides, a non-calibrated mass-spectrometer (MS) was used to follow ammonia desorption, giving us qualitative information about the strength distribution of acid sites. Additionally, acid sites present in our materials were also probed by FTIR measurements with adsorption-desorption of pyridine in a Nicolet Is-10 Thermo FT-infra-red spectrophotometer. In this case, acid site quantification has been done using the extinction coefficients given in ref. [43]. The reduction behaviour of copper in these materials was studied by a temperature-programmed reduction (TPR) analysis conducted in a Micromeritics Autochem 2910 equipment. About 30 mg were firstly fluxed with 30 cm^3/min of Ar at room temperature for 30 min, and then a mixture of 10 vol% of H_2 in Ar was passed through the sample at a total flow rate of 50 cm^3/min, while the temperature was increased up to 800 °C at a heating rate of 10 °C/min. The H_2 consumption rate was monitored in a thermal conductivity detector (TCD) previously calibrated using CuO reduction as reference. Copper dispersion in the silica-based materials was measured by N_2O titration by following the procedure described by Pakharukova et al. [44] The technique comprises three steps: reduction to Cu^0, oxidation of Cu^0 to Cu_2O using N_2O, and temperature-programmed reduction of Cu_2O surface species. 80 mg of sample were loaded in a glass flow microreactor. The reduction was carried out at the minimum temperature needed to completely reduce CuO to Cu^0. Reduced samples were cooled to 60 °C and exposed to N_2O for 45 min. The last TPR was done on the freshly oxidised Cu_2O surface up to 500 °C. H_2 uptake was followed with a thermal conductivity detector.

In this manner, copper dispersion (D_{Cu}), defined as a ratio of Cu exposed at the surface to total Cu, can be calculated by dividing the H_2 uptake from the second TPR (nH_2(TPR-2): mol H_2 / g catalyst) by the total amount of Cu determined by ICP analysis (n_{Cu}: mol Cu / g catalyst).

$$D_{Cu}(\%) = \frac{2nH_2(TPR - 2)}{n_{Cu}} \bullet 100 \tag{1}$$

The specific surface area of metallic copper (D_{Cu}) was calculated using the following expression:

$$S_{Cu}^{N_2O}(m^2/g) = \frac{M_{H_2}SFN_A}{10^4 C_M W_{Cu}} \tag{2}$$

where M_{H2}, SF, N_A, C_M, and W_{Cu} are moles of hydrogen consumed per unit mass of catalyst (μmol H2/g cat), stoichiometric factor (2), Avogadro's number (6.022×10^{23} mol^{-1}), number of copper atoms per unit surface area (1.46×10^{19} atoms·m^{-2}) and Cu content (wt%), respectively.

Also, by assuming a spherical shape of particles, the average size of copper particles ($S_{Cu}^{N_2O}$) was determined by the following expression:

$$d_{Cu}^{N_2O}(nm) = \frac{6 \bullet 10^3}{S_{Cu}^{N_2O} \bullet \rho_{Cu}} \tag{3}$$

where ρ is copper density (8.92 g/cm^3).

Thermogravimetric analyses (TG) were carried out in a Mettler Toledo TGA/SDTA 851 apparatus, using a heating rate of 10 °C/min in an airstream until 800 °C was reached. Elemental analysis (EA) was carried out in a Fisons EA1108CHN-S apparatus. Sulphanilamide was used as reference. These two techniques (TG and EA) were applied to determine and evaluate the organic content deposited on the catalyst surface throughout the reaction.

2.3. Catalytic experiments

Catalytic experiments were done in a vertical stainless-steel tubular fixed-bed reactor (length = 25 cm and diameter = 0.5 cm), with the catalyst (0.500 g) pelletized in particles of 0.425–0.600 mm in size diluted with SiC (0.600–0.800 mm). Typically, catalytic tests were carried out by feeding the reactor with a liquid mixture of glycerol and methanol (MeOH) (2 mL/h, 50:50 wt. ratio) at 240 °C and atmospheric pressure for at least 8 h. A Figure illustrating the reactor design can be found in the SI (Fig. S2). Additionally, results for calculations with the software ASPEN HYSIS applying the property package UNIQUAC – Ideal to an Equilibrium Reactor can be found in the SI (Fig. S3), providing information about the physical state of the reaction mixture under these conditions. Under these conditions, the experiments have been performed under strict kinetic limitations (Fig. S4). For each experiment, cumulative fractions (corresponding to 0–1 h, 1–2 h, 2–3 h, etc.) were collected in a glass recipient submerged in an ice bath at 2 °C. Considered as an induction-stabilisation time, in every case, the fraction from 0 to 1 h, although collected, was disregarded in average calculations.

A combination of two GC instruments analysed liquid samples. Most polar compounds were analysed with a Varian CP-3800, equipped with an FID detector and a CARBOWAX Column (15 m x 3.2 mm). On the other hand, non-polar compounds and the desired product (acetol) were determined with an Agilent Technologies 7890 A GC system with an FID detector equipped with an HP-5 MS capillary column (30 m x 250 μm x 0.25 μm). Figs. S5 and S6 illustrate typical chromatograms obtained in each case. In both cases, the internal standard methodology was employed to quantify the different components in the reaction mixture. Chlorobenzene (1 wt% in MeOH) was the internal standard used in the case of the HP-5 column, while 1,4-butanediol (1 wt% in MeOH) was the one selected in the analysis performed on the CARBOWAX column. Product identification was done by GC–MS (Agilent 6890 N GC System, with an HP-5 column) coupled with an Agilent 5973 N mass detector). Silylation with ethylacetate diluted N,O-Bis(trimethylsilyl) trifluoroacetamine with 1 wt% trimethylsililchloride (ACROS Organics) was carried out on some MeOH-previously evaporated samples to improve the identification of the most polar compounds in the HP-5 column. Figs. S7–S12 present the most important compounds

identified by GC-MS analysis.

In all cases, glycerol conversion (X), selectivities (S_i) and yields (Y_i) of the different products "i" have been calculated through the GC analysis of the different aliquots corresponding to different reaction times ("t"):

$$X_{glycerol}(mol.\%) = \frac{n^f_{glycerol}*}{n^0_{glycerol}} \cdot 100 \qquad (4)$$

*Polyglycerols not separated from the main glycerol chromatographic peak, observed at low glycerol conversions, are considered to be likely coming from glycerol condensation in the injection chamber and counted as glycerol.

$$Y^t_i(mol.\%) = \frac{n^t_i \bullet a_i}{n^0_{glycerol}} \cdot 100 \qquad (5)$$

Being a_i the stoichiometric correction factor for the product "i".

In particular, selectivity to acetol (and to the different products) was calculated both considering the amount of glycerol converted and as a function of the total amount of products in the liquid fraction:

$$S^T_{acetol}(mol.\%) = \frac{n^f_{acetol}}{n^0_{glycerol} - n^f_{glycerol}} \cdot 100 \qquad (6)$$

$$S^L_{acetol}(mol.\%) = \frac{n^f_{acetol}}{n^f_{liquidproducts}} \cdot 100 \qquad (7)$$

Carbon balances of the reaction with respect to the total amount of glycerol fed into the reactor were also calculated as follows:

$$CB_{glycerol}(mol\%) = \frac{\sum n^f_{product_i} \bullet x_i C \text{ atoms}}{n^0_{glycerol} \bullet 3C \text{ atoms}} \cdot 100 \qquad (8)$$

Being x_i the number of carbon atoms in the $product_i$ coming from glycerol reaction.

It is worth noting that MeOH also reacts under the above-described reaction conditions, producing mainly H_2 and other gaseous products. Consequently, the gas fraction has been disregarded in the calculations to assure sticking to the glycerol reaction. On the other hand, in the liquid phase, methyl-formiate was identified as coming exclusively from MeOH reaction and left aside in the calculations.

Finally, TON (Turnover Number) and SA (Specific Activity) were also calculated for glycerol dehydration and defined as mol of glycerol converted and mol of acetol produced per mol of Cu present in the catalyst, respectively.

$$TON = \frac{n^0_{glycerol} - n^f_{glycerol}}{n^0_{Cu}} \qquad (9)$$

$$SA = \frac{n^f_{acetol}}{n^0_{Cu}} \qquad (10)$$

For reusability tests, after reaction the solid catalyst was washed with 40 mL of MeOH (2 mL/min) in the same reactor at the reaction temperature, and then treated at 550 °C during 4 h in air flow (3 °C/min, 50 mL/min). Afterwards, the solid catalyst was again used in a new catalytic reaction (re-use). The catalytic experiments together with the analytics corresponding to the re-usability tests were performed in the same way as the common experiments already described.

3. Results and discussion

3.1. Characterisation of CuO supported on silica materials

The main physicochemical and textural properties of different CuO supported on silica materials here prepared are listed in Table 1. The analysis showed similar surface areas (ranging from 218 to 245 m²/g) and copper contents (between 5.0 and 5.8 wt%) for the different

Table 1
Main physicochemical and textural properties of different silica supported CuO materials.

| Catalyst	Cu loading (wt %)[a]	BET area (m²/g)[b]	Pore volume (cm³/g)[c]
CuO-IW/SiO₂-CH	5.0	219	0.92
CuO-PD/SiO₂-CH	5.8	242	0.73
CuO-PD/SiO₂-AL	5.8	218	0.92
CuO-AP/SiO₂-AL	5.8	245	0.71

[a]Calculated by ICP.[b,c] Calculated from N₂-adsorption isotherms data.

materials studied here after CuO incorporation. The fact that the surface area decreased more dramatically; from $\approx$ 300 m²/g (see Table S1) to $\approx$ 200–250 m²/g for SiO₂-AL after Cu incorporation might be ascribed to the different average pore sizes in each one of the supports (i.e., 13.0 nm for SiO₂-CH and 10.0 nm for SiO₂-AL). Probably, for SiO₂-CH, the nanoparticles would not be able to block most of the pores, whereas they would be more capable in the case of SiO₂-AL, with thinner pores. For comparison, CuO-PD/SBA-15, and CuO-IW/Al₂O₃ materials were also prepared, and their complete characterisation data can be found at the SI (Table S2 and Figs. S13–S17).

Fig. 1 shows the XRD patterns of the four CuO/SiO₂ catalysts containing $\approx$ 5 wt% copper. In all cases, SiO₂-based catalysts can be defined as having an amorphous structure. On the contrary, the differences provoked because of the presence of copper from one material to another are quite noticeable. In those materials in which the copper has been incorporated by the precipitation-deposition method (PD) and by a previous grafting with APTES (AP), the signals corresponding to copper (II) oxide are barely seen, while the material prepared by incipient wetness impregnation (IW) clearly shows the reflexions characteristics of CuO. These observations already reveal the higher dispersion of CuO achieved when using the precipitation-deposition method (PD) or a previous grafting with APTES (AP) against that obtained by incipient wetness (IW).

The four CuO/SiO₂ materials were also analysed by HR-TEM and HR-STEM measurements (Fig. 2), as well as N₂O titration method (see 2.2. Catalysts characterisation section). Thus, besides the qualitative information extracted from a quick analysis of the X-ray diffraction patterns, titration with N₂O and particle size distribution by STEM imaging were used to put concrete numbers to the metal oxide dispersion (Table 2). For CuO-IW/SiO₂-CH and CuO-PD/SiO₂-CH materials, there is a good agreement between the XRD, STEM and the N₂O titration data. Every technique shows the higher efficiency of the precipitation-deposition method (PD) to achieve higher dispersions than the incipient wetness
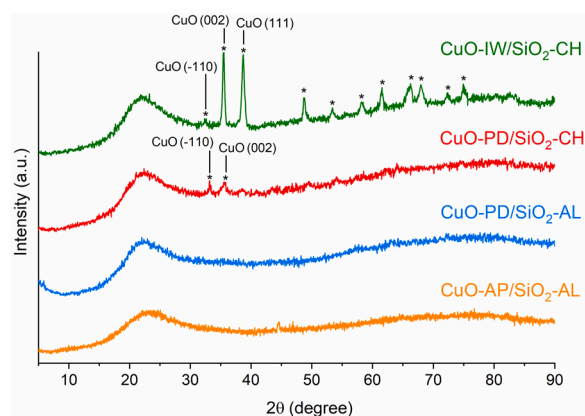
Fig. 1. Wide angle X-Ray powder diffraction patterns of CuO supported on SiO₂ materials. *: CuO (JCPDS: 00–045–0937).
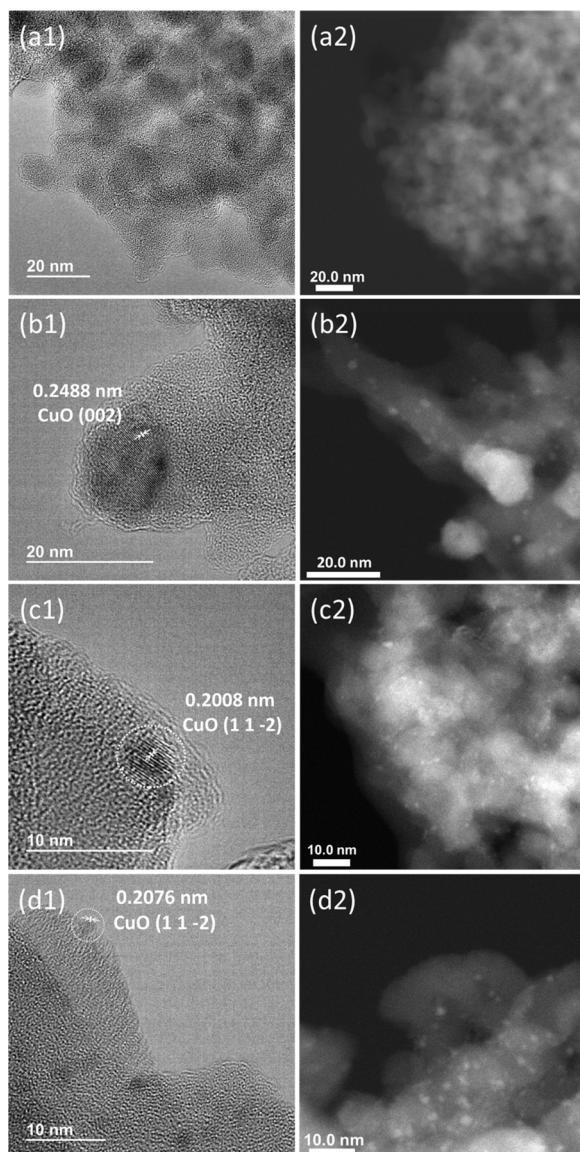
Fig. 2. (1) HR-TEM and (2) HR-STEM micrographs for (a) CuO-IW/SiO$_2$-CH, (b) CuO-PD/SiO$_2$-CH, (c) CuO-PD/SiO$_2$-AL and (d) CuO-AP/SiO$_2$-AL.

Table 2
CuO dispersion on several SiO$_2$ materials.

Catalyst	STEM Particle size (nm)[a,b]	N$_2$O titration Particle size (nm)[c]	Dispersion (m^2 Cu/ g Cu)[c]
CuO-IW/ SiO$_2$-CH	9.4 ± 6.8	6.1	110
CuO-PD/ SiO$_2$-CH	6.2 ± 10.6	4.8	142
CuO-PD/ SiO$_2$-AL	2.1 ± 1.5	2.9	233
CuO-AP/ SiO$_2$-AL	1.6 ± 0.6	3.2	213

[a] Average particle size measured by HR-STEM ± the 2σ value (a minimum number of 200 particles was considered).
[b] Particle size distributions obtained by analyses of STEM micrographs can be found at the SI (Fig. S18).
[c] Measured by surface N$_2$O oxidation of the reduced catalyst and subsequent reduction.

methodology (IW). Additionally, CuO-PD/SiO$_2$-AL presents higher dispersion and smaller particle size values (by both N$_2$O and STEM) than CuO-PD/SiO$_2$-CH, also in good agreement with the intensity of XRD peaks corresponding to CuO, which can be seen just for the former one. This fact was also predictable since SiO$_2$-AL is a SiO$_2$ with a larger surface area than the SiO$_2$-CH (Table S1), resulting in better dispersion of the CuO nanoparticles when incorporated by the same methodology. Last, although N$_2$O titration barely sees differences between CuO-PD/SiO$_2$-AL and CuO-AP/SiO$_2$-AL, STEM imaging shows that the incorporation of CuO by the previous functionalization of the silica surface (SiO$_2$-AL) with APTES (CuO-AP/SiO$_2$-AL) is the methodology giving rise to the smallest particle size values for the metallic oxide. In that direction, CuO-AP/SiO$_2$-AL is the only sample where this technique could not see particles above 3 nm (see Fig. S18).

Moreover, a study of the acidic properties of the four CuO/SiO$_2$ materials was conducted. First, we carried out FTIR-followed pyridine adsorption-desorption experiments. The first cycle of pyridine adsorption and desorption at 150 °C (Fig. S19) allowed us to confirm that Lewis acid sites are the ones that prevail for this family of materials, being the Brönsted acidity practically negligible. Moreover, the analyses unravel how, as reported by previous studies [36,37], the smaller the particle size, the larger the number of acid sites. However, the peaks' intensity and shapes make it difficult to discriminate between real Lewis acid centres and physiosorbed pyridine at higher temperatures. Consequently, the distinction between weak, medium, and strong acid centres is not reliable by this technique. Thus, to secure a better way to discriminate between the materials, a study of their acidic properties was carried out through adsorption and temperature-programmed desorption of ammonia (TPD-NH$_3$). The similar profiles for the qualitative desorption curves in Fig. S20, essentially reveal a similar strength for the acid sites displayed by these catalysts. Then, the main differences are observed in the quantity of ammonia adsorbed, that is to say, in the total number of acid sites. In this regard, Table 3 shows the total amount of ammonia adsorbed for each catalyst, and the same value but normalised by each of the catalyst surface areas, both columns pointing out the same trend. These data, congruent with the tendency observed by pyridine adsorption-desorption at 150 °C, allows for establishing important differences between the various materials, whose total acidity can be ordered as follows: CuO-AP/SiO$_2$-AL > CuO-PD/SiO$_2$-AL > CuO-PD/SiO$_2$-CH >> CuO-IW/SiO$_2$-CH. As can be seen, while acid sites offered by CuO-IW supported on SiO$_2$-CH are practically negligible, in the sample showing the smallest particle size and thinner dispersion (see Fig. S18) CuO-AP/SiO$_2$-AL, a considerable amount of Lewis acid sites is observed. The sites range mainly from weak to moderate acid strength in all cases. In this sense, as the acidity provided by the SiO$_2$ is, in effect, insignificant (see the FTIR-pyridine analyses for the supports, Table S1), all the differences in acidity can be attributed to the different nature of the Cu structures supported in each material. These findings are in good agreement with the previous observations made by N.

Table 3
Acid site measurements for different CuO supported on SiO$_2$ catalysts.

Catalyst	Acid sites (μmol PYR/g)[a]	Acid sites (μmol NH$_3$/g)[b]	Acid site density (μmol NH$_3$/m^2)[b,c]
CuO-IW/ SiO$_2$-CH	4	14	0.06
CuO-PD/ SiO$_2$-CH	41	83	0.34
CuO-PD/ SiO$_2$-AL	71	127	0.58
CuO-AP/ SiO$_2$-AL	99	279	1.14

[a] Measured by FTIR with pyridine (PYR) as probe molecule. Molar extinction coefficient from Ref. [42].
[b] Values calculated from NH$_3$-TPD measurements.
[c] Acid site density = Acid sites / surface area.

Ravasio and co-workers, stating that high copper oxide dispersions lead to increasing acidities [36,37].

Last, the redox features of the CuO/SiO₂ materials herein prepared were studied by XPS and TPR analyses (Fig. 3). Importantly, TPR traces of the materials prepared by those methods leading to higher dispersions, namely precipitation-deposition (PD) and grafting with APTES (AP), show an absolute maximum at ≈ 190 °C. On the contrary, the material prepared by using the incipient wetness impregnation methodology (CuO-IW/SiO₂-CH) displays its maximum at ≈ 225 °C. These maximums have already been reported to correspond to the complete reduction of Cu (Cu^{2+}→Cu^0) [45]. Importantly, these TPR graphs make sense when considering that higher CuO dispersions (i.e., smaller particle sizes) give rise to higher reducibilities [46,47].

On the other hand, XPS analyses were carried out for the whole series of materials with the primary objective of ascertaining the oxidation state of copper in each of the materials (Figs. 3b, and S21 and S22, and Table S3 in SI). Interestingly, the ratio between Cu2p$_{3/2}$ satellite and main peak allowed us to identify Cu(II) as the prevalent oxidation state in all cases. However, there is a shift towards higher BE (≈ 935 eV) for those samples with higher dispersion (with the reduction peak at lower temperatures) with respect to the value observed for the sample with the lower dispersion and reducibility (≈ 933 eV). Most literature studies of similar systems have ascribed the peak at 935 eV to Cu-O-Si-O-, and the one at 933 eV to CuO [48–51]. Interestingly, the same support SiO₂-CH presents a total absence of the XPS signal corresponding to Cu-O-Si-O when copper is incorporated by the incipient wetness impregnation method (CuO-IW/SiO₂-CH), whereas its maxima corresponds with this linkage when incorporated by the precipitation deposition method (CuO-PD/SiO₂-CH). Therefore, the formation of Cu-O-Si-O is more likely to be related to the dispersion degree achieved rather than with the surface properties of the bare support. Indeed, the fact that higher dispersions favour these linkages is in good agreement with some prior authors' claims about Cu-O-Si-O- being produced on the interface of nanoscale copper species and SiO₂ [51]. In this line, smaller nanoparticles would mean higher interface areas and, therefore, larger Cu-O-Si-O- abundance.

In the direction of what has been observed by XPS, it is worth noting that the recent article by W. Fan and co-workers [51] also points out that these Cu-O-Si-O- structures should act as either primary active sites or precursors [52] for those active Cu(I) sites involved in the glycerol dehydration to acetol. In addition, as previously stated in the introduction, some authors even ascribe the enhanced acidity of the

CuO/SiO₂ system to an augmented presence of Cu-O-Si-O moieties.

Summarising, as a consequence of the different syntheses already described in Section 2.1, a family of silica supported CuO materials were attained where significant differences in the particle sizes of CuO could be observed. Interestingly, higher dispersion (smaller particle sizes) brings with it an increase in the metal active area, higher total acidities, higher reducibilities and the generation of distinct Cu species.

3.2. Catalytic activity

Initially, to spotlight the interest of the study herein described, the catalysts CuO-IW/Al₂O₃ and CuO-IW/SiO₂-CH, analogous to some of those already reported in the literature [33], and with similar CuO particle sizes, were tested in the selective dehydration of glycerol to acetol by using a continuous flow fixed-bed reactor system. The reaction conditions employed (feed = methanol/glycerol, 50/50 in weight, flow = 2 mL/h, with 0.5 g catalyst, particle size = 0.425–0.600 mm, at 240
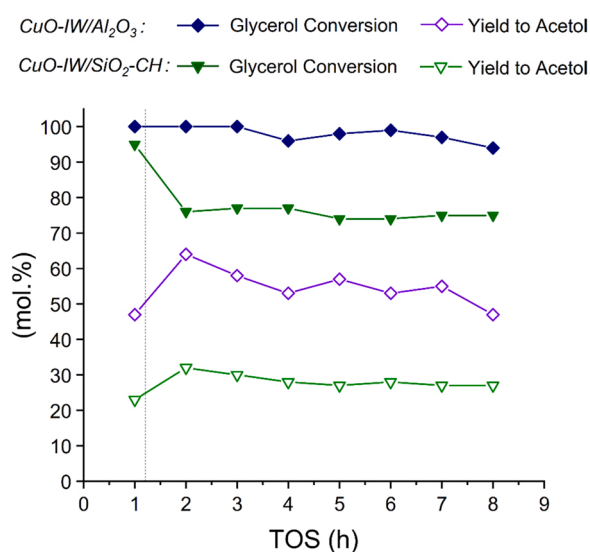

Fig. 4. Catalytic comparison between CuO-IW/SiO₂-CH and CuO-IW/Al₂O₃. Reaction conditions: feed = methanol/glycerol (50/50 in weight), flow = 2 mL/h, with 0.5 g catalyst (0.425–0.600 mm), at 240 °C, TOS = 8 h.
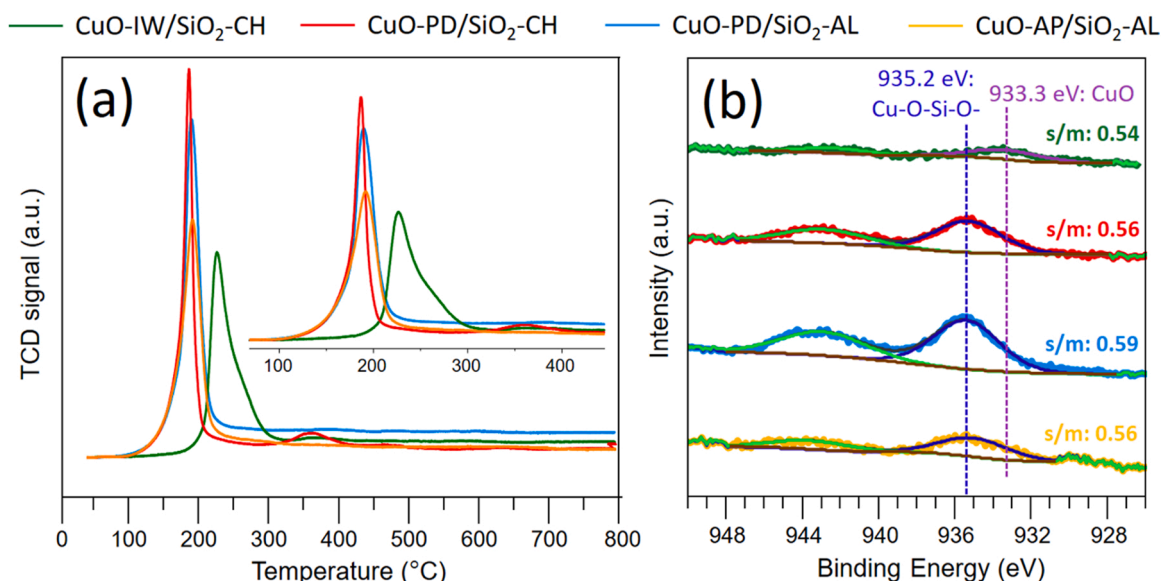

Fig. 3. (a) TPR traces and (b) Cu2p$_{3/2}$ XPS region for CuO supported on SiO₂ materials.

°C, TOS = 8 h) were those which were going to be used throughout the present work. Comparative catalytic results expressed in terms of glycerol conversion and acetol yield for both CuO-IW/Al₂O₃ and CuO-IW/-SiO₂-CH are depicted in Fig. 4. As can be seen, average glycerol conversion higher than 90% with acetol yield around 60% can be reached with CuO-IW/Al₂O₃ catalyst, whereas much lower both glycerol conversion (<80%) and acetol yield (≈30%) are achieved with CuO-IW/SiO₂-CH sample. Interestingly, this first example already highlights the problem of lacking acid centres to enhance acetol production. The material CuO-IW/Al₂O₃ possesses a significant amount of acid centres per gram (99 μmol NH₃/g), whereas CuO-IW/SiO₂-CH barely shows any significant acidity (14 μmol NH₃/g). Moreover, this difference becomes even more pronounced when the amount of acid sites is normalised by the surface area of the materials (0.76 vs 0.06 μmol NH₃/m², respectively). As it has already been mentioned and explained elsewhere [33], the absence of acidity results in a material that cannot successfully interact with glycerol, which brings about a catalyst with lower activity and lower selectivity to the desired acetol (CuO-IW/SiO₂-CH, 9.4 nm by STEM), when compared with a material showing a similar amount of exposed CuO (CuO-IW/Al₂O₃, 8.4 nm by STEM).

Hence, this finding raises the issue of whether introducing some acidity in the CuO/SiO₂ used as catalyst could be possible, to boost acetol production. Instead of functionalizing the SiO₂, which could be an alternative approach, the decision was made to decrease the particle size

of CuO, thereby achieving a double effect consisting of increasing the active surface area and taking advantage of the already reported acidity arising in these systems when improving copper oxide dispersion [36, 37]. With this aim, and according to the characterisation section, a series of materials having different CuO particle sizes and, therefore, different acidities, were successfully prepared (see Section 3.1). These materials, namely CuO-IW/SiO₂-CH, CuO-PD/SiO₂-CH, CuO-PD/SiO₂-AL, CuO-AP/SiO₂-AL, were tested in the catalytic dehydration of glycerol to acetol, and the results are illustrated in Fig. 5. Fig. 5a shows the cumulative data for glycerol conversion, yield to the different products, and carbon balance in the dehydration of glycerol for a time on stream (TOS) between 1 and 8 h. In contrast, Fig. 5b represents the cumulative selectivity to acetol and Fig. 5c and d show glycerol conversion and selectivity to acetol as a function of TOS for the different CuO/SiO₂ materials herein prepared. As can be seen, the best results were attained with the CuO-PD/SiO₂-AL and CuO-AP/SiO₂-AL, with the practically total conversion of glycerol (≈100%), yield to liquid products ≈ 80% (Acetol + 1,2-PDOs + Acid & Esters + Others), and selectivity to acetol up to 70% in the liquid fraction. Every graph shows how the smaller the CuO particle size, the higher activity and selectivity towards the desired acetol, being this effect very significant when comparing CuO-PD/-SiO₂-AL (2.9 nm, by N₂O) and CuO-AP/SiO₂-AL (3.2 nm, by N₂O) with CuO-PD/SiO₂-CH (4.8 nm, by N₂O) and, especially with CuO-IW/-SiO₂-CH (6.1 nm, by N₂O). Consequently, results suggest that those materials exhibiting higher acidity and preferable prepared by methods
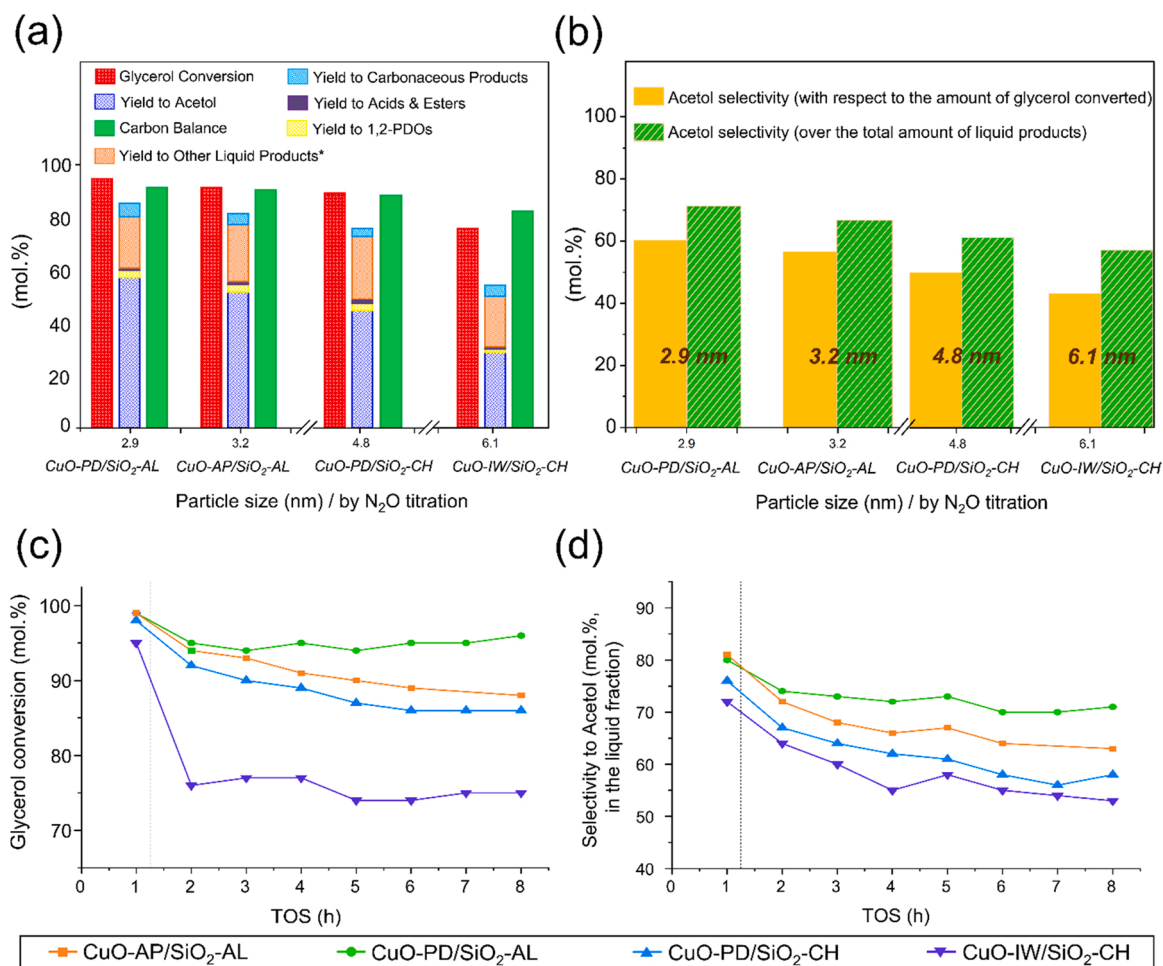

Fig. 5. Cumulative (a) glycerol conversion, yield to liquids and carbon balance, (b) Acetol selectivities, (c) Glycerol conversion vs time on stream, and (d) Acetol selectivity vs time on stream for the dehydration of glycerol over different CuO supported on SiO₂ catalysts. Reaction conditions: feed = methanol/glycerol (50/50 in weight), flow = 2 mL/h, with 0.5 g catalyst (0.425–0.600 mm), at 240 °C, TOS = 8 h. *Other liquid products: acetoin, acetoin methyl ether, 3-methoxybutanol, hydroxyacetone dimethyl acetal, solketal and other unidentified by-products.

providing a higher degree of dispersion (and generating smaller particles size) for the copper oxide, such as the precipitation-deposition method (PD) and the grafting with APTES (AP), are more capable of attaining better results. Regarding the explanation of the much more subtle catalytic differences between them, it seems that the presence of a considerably larger number of acid sites (and amounts of nanoparticles detected by STEM imaging) observed in CuO-AP/SiO₂-AL with respect to CuO-PD/SiO₂-AL is having a substantial effect on the catalytic activity, which could consist of stronger adsorption of acetol [29], leading to lower selectivities and a more pronounced catalyst deactivation (Fig. 5c).

Excitingly, glycerol conversion (≈100%) and yield to acetol (≈60%) reached with our best CuO/SiO₂ catalyst (CuO-PD/SiO₂-AL) become close to those achieved by using CuO-IW/Al₂O₃ catalyst (see Fig. 6). In light of these results, the use of highly dispersed CuO-supported on silica materials becomes an excellent choice to build up efficient catalytic systems, which might be useful and economical alternatives for the selective dehydration of glycerol. The higher Cu dispersion and the introduction of acidity needed for the first glycerol adsorption [29,33], appear to be the cause for this improved catalytic activity. In fact, the enhancement in Cu dispersion allowed us to work with a CuO-based material with less acidity than that observed for the CuO-IW/Al₂O₃ catalyst (0.58 vs 0.76 μmol NH_3/m^2), thus helping to avoid non-desired by-products (Table S4).

The fact that the activity of a CuO/SiO₂ sample, this meaning Cu species supported onto non-acidic silica, is close to or comparable to CuO/Al₂O₃ material becomes itself an exemplary behaviour, a relevant result, and an interesting scientific output, not reported up to now for this process when using this heterogeneous catalyst composed by copper, silicon and oxygen. In this sense, and due to our catalyst optimisation, it is possible to overcome the results previously reported in which CuO/SiO₂ was used as catalyst for this reaction. For instance, the most similar try was done so far by Xiaofei et al. [53], reporting a glycerol conversion of 99% and a selectivity to acetol of 58% as the best result. Nonetheless, reaction temperature was above ours (300 °C), and the productivity was much lower, i.e., WHSV = 1.4 h⁻¹ and glycerol mass fraction 20% vs WHSV = 4.0 h⁻¹ and 50% glycerol in our case, respectively. Additionally, they reached shorter times on stream (6 h) and the Cu content in the catalyst was also significantly higher (20 wt%). On the

other hand, Sato et al.[27], reported results for CuO/SiO₂ far below those observed in our work (≈23% yield to acetol), even although a hydrogen pre-activation of the catalyst was performed.

3.3. Structure-activity relationships

Fig. 7 depicts (a) the correlation between acidity and the particle size of the CuO nanoparticles and (b) the behaviour of each catalyst in terms of acetol production per Cu site in that period when no catalyst has started to suffer from any significant deactivation (TOS = 1–4 h). The tendency mentioned above, consisting of an increase in the acidity if improving the CuO dispersion, is well illustrated in Fig. 7a. Both particle size measurements (STEM imaging and N₂O titration) fit reasonably well with exponential curves when representing the acid site density with respect to them. Interestingly, the effect of reducing the CuO particle size on the catalytic activity and, at the same time, increasing the acidity coincides with an improvement of the acetol production rate per mol of Cu present in the catalyst (Fig. 7a), which ends up achieving close yields to the reference catalyst CuO-IW/Al₂O₃ (Fig. 6). The enhancement in the acetol production rate with the amount of Cu exposed (i.e., CuO particle size) adjusts quite well to a linear fit (Fig. 7b, purple trace). Additionally, Fig. 7b shows an opposite trend when increasing the number of acid sites per unit area or acid site density (green trace). However, an asymptotic tendency is observed in this case, probably meaning that excessively high concentrations of acid sites could unpair the specific activity towards producing the desired acetol.

At this stage, it would be possible to ascribe the upgrading in the acetol production rate to three different factors: 1) an increase in the amount of Cu exposed, 2) an increase in the number of acid sites per area unit, but also to 3) an intrinsically superior activity of those Cu sites which are present in smaller CuO nanoparticles. To assess the third point, a comparison should be made by considering the amount of CuO exposed in every case (see Fig. S23). When considering the amount of acetol produced by only those Cu atoms that are truly accessible to the substrate, it appears to be a maximum at particles sizes around 10 nm. Accordingly, it seems that those Cu sites present when there are nanoparticles around 10 nm exhibit an equal if not superior intrinsic activity to carry out the glycerol dehydration to acetol than those present in systems with smaller CuO particle sizes. In that line, the reducibility
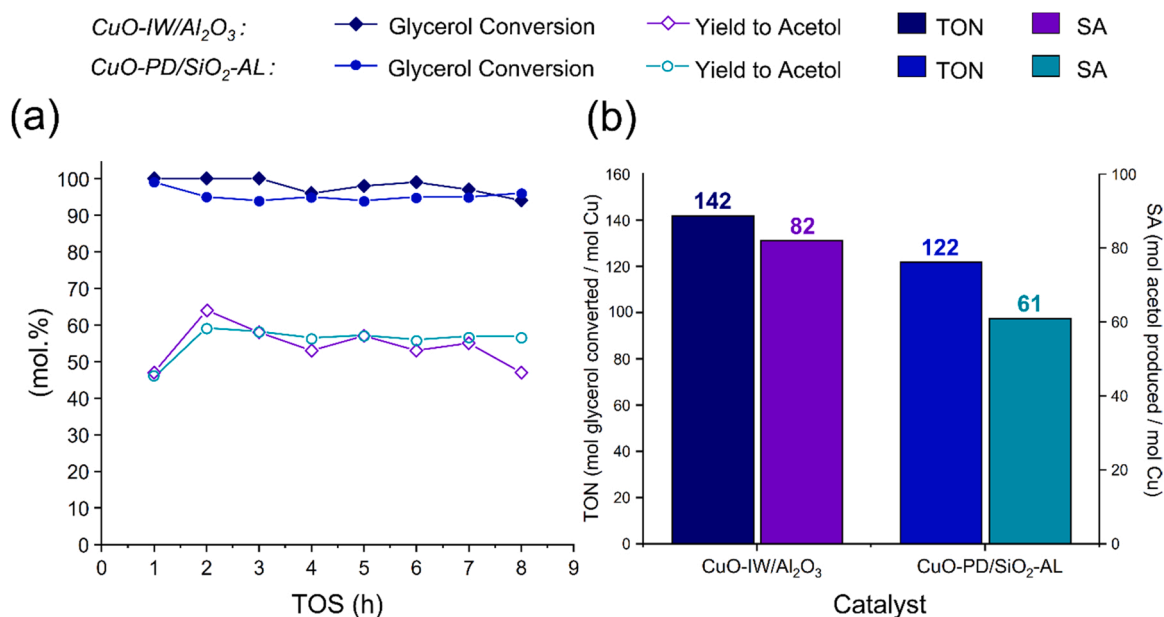

Fig. 6. (a) Catalytic comparison between CuO-PD/SiO₂-AL and CuO-IW/Al₂O₃. (b) Average TON and Specific Activity (SA) for CuO-PD/SiO₂-AL and CuO-IW/Al₂O₃ when working with lower catalyst loadings (i.e., lower conversion level, <100%). Reaction conditions: feed = methanol/glycerol (50/50 in weight), flow = 2 mL/h, with (a) 0.5 g or (b) 0.25 g catalyst (0.425–0.600 mm), at 240 °C, TOS = 8 h (a) = 4 h (b).
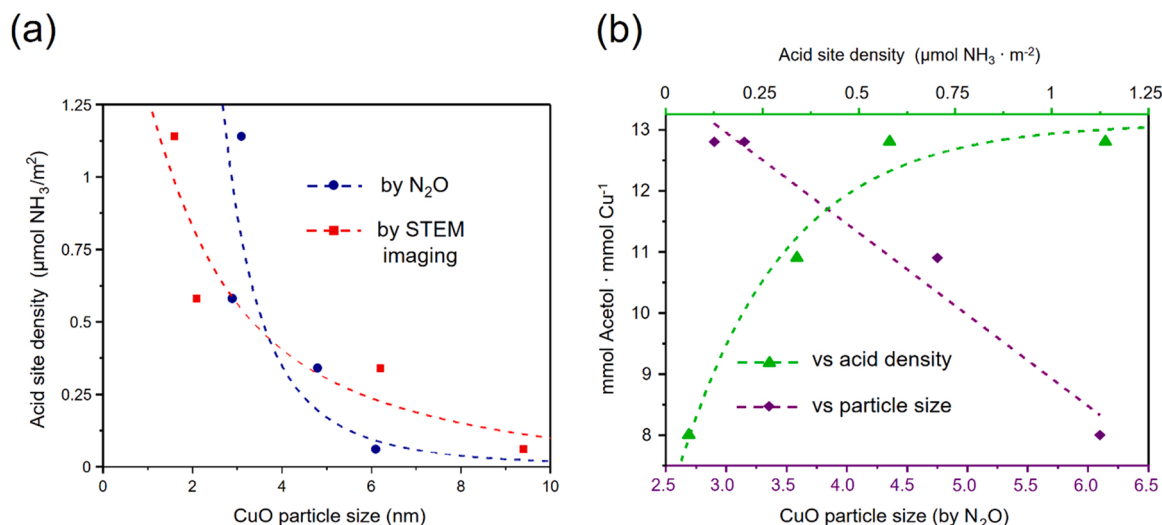
J. Mazarío et al.

Applied Catalysis A, General 652 (2023) 119029

Fig. 7. (a) Correlation between acid site density and CuO particle size. (b) Specific activities (SA) towards the acetol production calculated based on total amount of Cu (ICP). Reaction conditions: feed = methanol/glycerol (50/50 in weight), flow = 2 mL/h, with 0.5 g catalyst (0.425–0.600 mm), at 240 ºC, at TOS = 1–4 h.

behaviour observed in Section 3.1 unravels that every system has a reduction temperature below the reaction temperature, and we previously demonstrated that, therefore, every system is in with a chance of generating reduced Cu species. However, in our previous work we could corroborate that, although the reducing character of the reaction mixture generates Cu^{1+} and Cu^0 species throughout the process, Cu^{1+} are the majority, the more active and the crucial ones to carry out this reaction [29,30].

Interestingly, the catalyst CuO-IW/SiO$_2$-CH is the only one where the moiety Cu^{II}-O-Si-O- was not the prevalent Cu structure detected by XPS (see Fig. 3b, and Table S3). According to the recent article by W. Fan and co-workers [51], one would expect a lower activity in a catalyst where these linkages are not prevalent, which are believed to be precursors of Cu(I) species [53]. Indeed, CuO-IW/SiO$_2$-CH displays not only the lowest glycerol conversion, but also the lowest acetol selectivity (Fig. 5).

Nonetheless, these results should not discard or confirm any previous assumption related to the Cu active species [29,30,51]. In this sense, further research must be conducted to follow the evolution of the copper species and study the evolution and connection between Cu^{II}-O-Si-O-, CuO, Cu$_2$O, and Cu^I-O-Si-O species throughout the catalytic process, which is beyond the scope of this work.

The finding concerning the intrinsic activity of CuO nanoparticles with different sizes supports the other two factors 1) an increase in the amount of Cu exposed, and 2) an increase in the number of acid sites per unit area, as the leading causes for the improvement achieved in this work. In that direction, Fig. 7b (purple trace) provides clear proof of an enhancement in the acetol production rate during glycerol dehydration with the amount of copper exposed that correlates with CuO particle size and dispersion. In fact, copper dispersion has recently been reported to be a sensitivity descriptor for the activity [33] and we also found it to be strongly related with the presence of Cu-O-Si-O linkages. Moreover, the need for acidity to allow for a first interaction glycerol – catalyst, well acknowledged in previous studies [29,33], has also been reinforced in this work by comparing the catalytic behaviour of CuO-IW/SiO$_2$-AL and CuO-IW/Al$_2$O$_3$ catalysts. Thus, it can be concluded that the two main reasons for this catalytic boost observed in CuO-supported on silica materials are the number of exposed Cu active sites, larger for smaller nanoparticles, together with the presence of the acidity generated in the CuO nanoparticles onto an intrinsically non-acidic support when decreasing their particle size, as reported by the literature [36,37].

3.4. Catalyst reusability

Since the CuO-PD/SiO$_2$-AL catalyst showed a high catalytic activity complemented with good selectivity to acetol in the selective dehydration of glycerol in a continuous flow fixed bed reactor, it was necessary to test whether the material could be used several times in the reaction. To address this issue, catalyst re-cycle was carried out by washing the catalyst used in the reaction with MeOH and then regenerating it under an air stream, thus introducing a thermal regeneration treatment between catalytic cycles (see Section 2.3). Fig. 8a shows the catalyst recycling results by comparing glycerol conversion and acetol yield over time on stream (TOS ≈ 11 h) by using a fresh and a firstly used and regenerated catalyst consecutively. As can be seen, both glycerol conversion and acetol yield suffer from certain decline after the first catalytic cycle.

As observed from the data of Fig. 8a, the loss of activity observed at TOS ≈ 11 h for the fresh catalyst could not be completely overcome by thermal regeneration. Although the drop over the first use was expected because of the deposition of organic matter on the catalytic surface, the elemental analysis studies unveiled (Table 4) that heating up to 550 ºC is enough to eliminate this carbonaceous material. Remarkably, no Cu leaching was observed for the selected material, as happened in all the CuO/SiO$_2$ materials so far tested, and a minor surface area loss was observed in every case (Table 4 and S5). In addition, glycerol conversion was practically re-established (Fig. 8a), although the acetol production was not fully recovered after the regeneration process. Importantly, STEM imaging analysis and N$_2$O titration reveal how, when subjecting the material to the reaction conditions followed by a thermal regeneration treatment, the average size of the CuO nanoparticles significantly increases (Fig. 8b and Table 4). In consonance with the CuO nanoparticle growth, the XPS of the used catalyst after regeneration shows a shift from 335.2 to 333.9 eV for the Cu2$p_{3/2}$ main peak, with respect to the fresh material, meaning a significant disappearance of Cu-O-Si-O linkages (Fig. 8c). These findings could account for this observed loss of activity.

3.5. Effect of introducing mesoporosity

Additional studies were done to improve the best catalyst CuO-PD/SiO$_2$-AL encountered for the selective dehydration of glycerol to acetol (glycerol conversion ≈100%, acetol yield ≈60%). In that direction, mesoporous silica could offer an additional opportunity to enhance the stability of highly dispersed CuO nanoparticles. Therefore, copper was

9
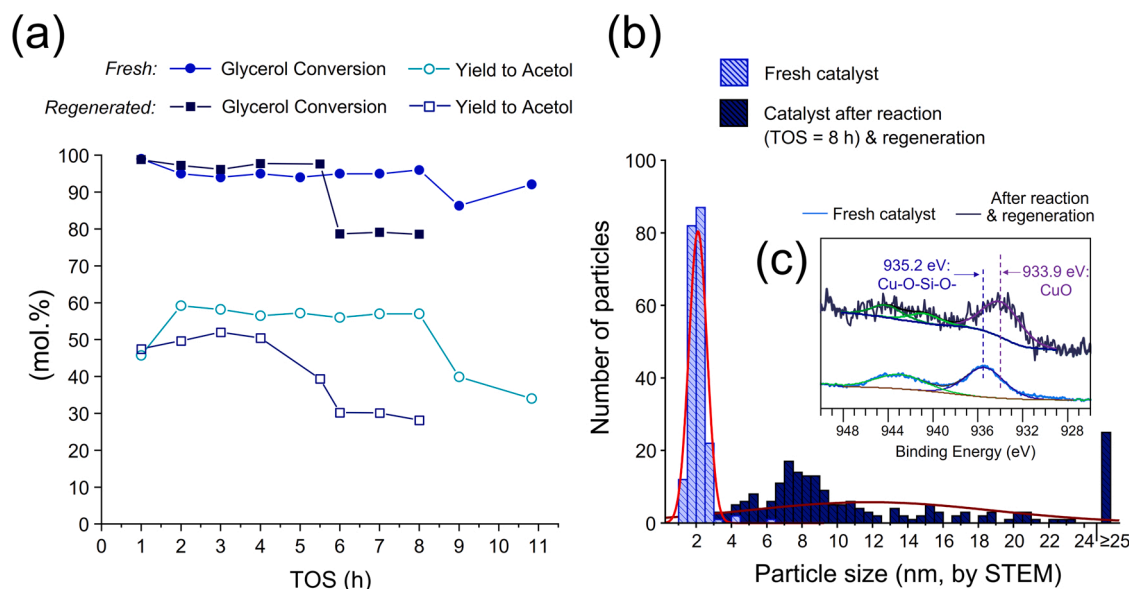
Fig. 8. (a) Glycerol conversion and yield to acetol with CuO-PD/SiO$_2$-AL over two consecutive catalytic cycles. (b) CuO particle size and (c) Cu2$p_{3/2}$ XPS region evolution over the reaction + regeneration process (STEM imaging) for CuO-PD/SiO$_2$-AL.Reaction conditions: feed = methanol/glycerol (50/50 in weight), flow = 2 mL/h, with 0.5 g catalyst (0.425–0.600 mm), at 240 °C.

Table 4
Effect of use (at TOS = 8 h) and regeneration on metal loading, surface area, organic matter deposition and metallic dispersion for CuO-PD/SiO$_2$-AL.

Physicochemical property	Fresh CuO-AP/SiO$_2$-AL	Used CuO-AP/SiO$_2$-AL	Regenerated[a] CuO-AP/SiO$_2$-AL
Cu loading (wt%)[b]	5.8	n/d	5.9
BET Area (m^2/g)[c]	218	n/d	181
Organic matter (wt %)[d]	–	26.5	0.3
STEM Particle size (nm)[e]	2.1 ± 1.5	n/d	14.6 ± 30.0
N2O Particle size (nm)[f]	2.9	n/d	7.6

[a] Washed with 40 mL of MeOH (2 mL min^{-1}) in the same reactor at the reaction temperature, then treated at 550 °C during 4 h in air flow (3 °C min^{-1}, 50 mL min^{-1}).
[b] Calculated by ICP.
[c] Calculated from N$_2$-adsorption isotherms data (BET method).
[d] Total amount of carbonaceous matter on the catalyst (measured by TGA).
[e] Average particle size measured by HR-STEM ± the 2σ value (a minimum number of 200 particles was considered).
[f] Measured by surface N$_2$O oxidation of the reduced catalyst and subsequent reduction.

incorporated by the precipitation-deposition method to pure mesoporous silica (SBA-15). The aims were to provide the system with active CuO nanoparticles mainly inside the silica pores to notably heighten catalyst stability by limiting Cu particle growth compared to catalysts with CuO deposited in amorphous SiO$_2$ materials, which are highly interconnected structures, and with unconstrained porosities. The results obtained for the catalytic dehydration of glycerol over these catalysts are given in Fig. 9. For comparative purposes, data reached with CuO-IW/Al$_2$O$_3$ reference catalyst for glycerol dehydration under reaction conditions herein employed are also included in Fig. 9.

The CuO-PD/SBA-15 has similar CuO nanoparticle sizes to CuO-PD/SiO$_2$-AL (2.1 ± 1.5 vs 3.0 ± 1.1 nm). However, and as can be concluded from catalytic results (Fig. 9), the mesoporosity of the silica matrix is a feature that has proved to have a detrimental effect on the yield of liquid products. Therefore, although the acid site density is lower than in the case of CuO-PD/SBA-15 (0.39 vs 0.58 mol NH$_3$/g), the mesoporosity of the silica matrix is likely to be the cause of the generation of more heavy
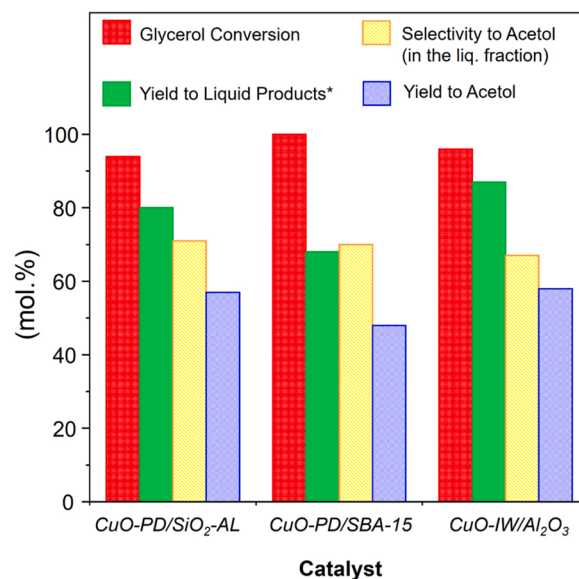
Fig. 9. Cumulative results in the glycerol dehydration for CuO-supported by precipitation-deposition (PD) materials compared to CuO-IW/Al$_2$O$_3$ (ref. catalyst). Reaction conditions: feed = methanol/glycerol (50/50 in weight), flow = 2 mL/h, with 0.5 g catalyst (0.425–0.600 mm), at 240 °C, TOS = 8 h. *Sum of all yields of the products present in the reaction mixture and detected by GC.

carbonaceous by-products, thereby decreasing the overall selectivity to acetol. Considering this decline in the catalytic results with respect to the CuO-PD/SiO$_2$-AL no further tests were done with mesoporous silica matrixes.

4. Conclusions

This research indicates that a waste by-product glycerol from biodiesel production can be transformed into acetol efficiently using an environmentally friendly Cu-supported silicon oxide catalyst. First, these results prove that, by taking advantage of the influence of the textural properties of the support and the copper incorporation

methodology, it is possible to prepare a family of materials with a wide range of CuO particle sizes. The acidity of these catalytic systems can be tuned by modifying the copper oxide dispersion by controlling CuO deposition and the type of silica used. By doing so, the copper oxide provides the system with the essential redox activity to carry out the reaction and the necessary acidity to interact with glycerol. The activity enhancement observed with CuO-supported on silica catalysts is mainly due to the number of exposed Cu active sites, larger for smaller nano-particles, together with the presence of the acidity generated in the materials when decreasing the CuO particle size. In addition, the in-crease in the acetol selectivity is likely to be explained because of the presence of a higher number of Cu-O-Si-O linkages, previously reported to be precursors for Cu(I). These Cu(I) species had already been iden-tified as the key species to successfully activate glycerol towards the desired acetol.

Thus, the material CuO-PD/SiO$_2$-AL displays a higher acetol yield than most catalysts already reported in the literature. Interestingly, the reaction is carried out in a continuous flow fixed-bed reaction system with a high concentration of glycerol in the feed at moderate operational conditions, favouring its scaling-up from an industrial viewpoint.

Nonetheless, although the copper content remains unchanging after use and regeneration, the stabilisation of the small copper oxide parti-cles poses a challenge that must be overcome to take advantage of the full potential of these catalytic systems. At this point, metal oxide nanoparticle growth associated to the loss of Cu-O-Si-O- linkages rep-resents a major deactivation mechanism over the SiO$_2$ supports. Consequently, its understanding and prevention are essential for designing catalysts with analogous compositions having longer lifetimes under current operation and regeneration conditions.

CRediT authorship contribution statement

J.M. and M.E.D conceived and designed the research work, including experiments, written the original draft and reviewed and edited the manuscript; J.M. performed the catalytic experiments, catalysts prepa-ration and catalysts characterisation, as well as the analysis of data; J.A. C. and E.R.C. performed some catalysts preparation and characterisa-tion, and helped in the analysis of data; M.E.D contributed with re-sources (reagents/materials and analysis tools) and funding, also supervising the investigation. All authors have read and agreed to the published version of the manuscript.

Declaration of Competing Interest

The authors declare the following financial interests/personal re-lationships which may be considered as potential competing interests: Marcelo E. Domine reports administrative support, article publishing charges, equipment, drugs, or supplies, and travel were provided by Institute of Chemical Technology. None.

Data availability

Data will be made available on request.

Acknowledgements

Appendix A. Supplementary material

Supplementary data associated with this article can be found in the online version at doi:10.1016/j.apcata.2023.119029.

References

[1] M. Stöcker, Angew. Chem. Int. Ed. 47 (2008) 9200.
[2] A. Demirbas, Energy Convers. Manag. 50 (2009) 2239–2249.
[3] G.W. Huber, S. Iborra, A. Corma, Chem. Rev. 106 (2006) 4044.
[4] G.W. Huber, A. Corma, Angew. Chem. Int. Ed. 46 (2007) 7184–7201.
[5] J.N. Chheda, G.W. Huber, J.A. Dumesic, Angew. Chem. Int. Ed. 46 (2007) 7164–7183.
[6] A.L. Moreira, J.M. Dias, M.F. Almeida, M.C. Alvim-Ferraz, Energy Fuels 24 (2010) 5717–5721.
[7] J. Costa, M. Almeida, M. Alvim-Ferraz, J. Dias, Energy Convers. Manag. 74 (2013) 17–23.
[8] S.C. D'Angelo, A. Dall'Ara, C. Mondelli, J. Pérez-Ramírez, S. Papadokonstantakis, ACS Sustain. Chem. Eng. 6 (2018) 16563–16572.
[9] G.M. Lari, G. Pastore, M. Haus, Y. Ding, S. Papadokonstantakis, C. Mondelli, J. Pérez-Ramírez, Energy Environ. Sci. 11 (2018) 1012–1029.
[10] D.T. Johnson, K.A. Taconi, Environ. Prog. 26 (2007) 338–348.
[11] C.C. Zhou, J.N. Beltramini, Y. Fan, G.M. Lu, Chem. Soc. Rev. 37 (2008) 527–549.
[12] J.C. Beltrán-Prieto, K. Kolomazník, J. Pecha, Aust. J. Chem. 66 (5) (2013) 511–521.
[13] N. Razali, A.Z. Abdullah, Appl. Catal. A Gen. 543 (2017) 234–246.
[14] D. Sun, Y. Yamada, S. Sato, W. Ueda, Appl. Catal. B Environ. 193 (2016) 75–92.
[15] S. Kandasamy, S.P. Samudrala, S. Bhattacharya, Catal. Sci. Technol. 9 (3) (2019) 567–577.
[16] A. Talebian-Kiakalaieh, Nor Aishah, S. Amin, H. Hezaveh, Renew. Sustain. Energy Rev. 40 (2014) 28–59.
[17] W.K. Teng, G.C. Ngoh, R. Yusoff, M.K. Aroua, Energy Convers. Manag. 88 (2014) 484–497.
[18] A. Martin, A. Richter, Eur. J. Lipid Sci. Technol. 113 (1) (2011) 100–117.
[19] A.R. Trifoi, P.Ş. Agachi, T. Pap, Renew. Sustain. Energy Rev. 62 (2016) 804–814.
[20] M.R. Nanda, Y. Zhang, Z. Yuan, W. Qin, H.S. Ghaziaskar, C.C. Xu, Renew. Sustain. Energy Rev. 56 (2016) 1022–1031.
[21] L. Hermida, H. Amani, S. Saeidi, A.Z. Abdullah, A.R. Mohamed, Rev. Chem. Eng. 34 (2) (2018) 239–265.
[22] B. List, J. Am. Chem. Soc. 122 (2000) 9336.
[23] W. Notz, B. List, J. Am. Chem. Soc. 122 (2000) 7386.
[24] M. Mazarío, Z. Raad, P. Concepción, C. Cerdá-Moreno, M.E. Domine, Catal. Sci. Technol. 10 (2020) 8049–8063.
[25] M. Dasari, P.-P. Kiatsimkul, W. Sutterlin, G. Suppes, Appl. Catal. A Gen. 281 (1–2) (2005) 225–231.
[26] C. Chiu, M.A. Dasari, G.J. Suppes, W.R. Sutterlin, AIChE J. 52 (2006) 3543.
[27] S. Sato, M. Akiyama, R. Takahashi, T. Hará, K. Inui, M. Yokota, Appl. Catal. A Gen. 347 (2008) 186–191.
[28] M. Velasquez, A. Santamaria, C. Batiot-Dupeyrat, Appl. Catal. B Environ. 160 (2014) 606.
[29] J. Mazarío, P. Concepción, M. Ventura, M.E. Domine, J. Catal. 385 (2020) 160–175.
[30] S. Célerier, S. Morisset, I. Batonneau-Gener, T. Belin, K. Younes, C. Batiot-Dupeyrat, Appl. Catal. A Gen. 557 (2018) 135–144.
[31] C. Montassier, D. Giraud, J. Barbier, Polyol conversion by liquid phase heterogeneous catalysis over metal, in: M. Guisnet, J. Barrault, C. Bouchoule, D. Duprez, C. Montassier, G. Pérot (Eds.), Studies in Surface Science and Catalysis, Elsevier, Poitiers, 1988, pp. 165–170.
[32] R.B. Mane, C.V. Rode, Green Chem. 14 (2012) 2780–2789.
[33] R.J. Chimentão, P. Hirunsit, C.S. Torres, M.B. Ordoño, A. Urakawa, J.L.G. Fierro, D. Ruiz, Catal. Today (2020).
[34] T.P. Braga, N. Essayem, S. Prakash, A. Valentini, J. Braz. Chem. Soc. 27 (2016) 2361–2371.
[35] T.P. Braga, N. Essayem, A. Valentini, RSC Adv. 5 (2015) 93394–93402.
[36] F. Zaccheria, N. Scotti, M. Marelli, R. Psaro, N. Ravasio, Dalton Trans. 42 (2013) 1319–1328.
[37] F. Zaccheria, N.I. Shaikh, N. Scotti, R. Psaro, N. Ravasio, Top. Catal. 57 (2014) 1085–1093.
[38] R.-P. Ye, L. Lin, C.-Q. Liu, C.-C. Chen, Y.-G. Yao, ChemCatChem 9 (24) (2017) 4587–4597.
[39] P.F. Fulvio, S. Pikus, M. Jaroniec, J. Mater. Chem. 15 (2005) 5049–5053.
[40] G. Díaz, R. Pérez-Hernández, A. Gómez-Cortés, M. Benaissa, R. Mariscal, J.L. G. Fierro, J. Catal. 187 (1) (1999) 1–14.
[41] Z. Huang, F. Cui, H. Kang, J. Chen, C. Xia, Appl. Catal. A 366 (2) (2009) 288–298.
[42] J. Rouquerol, P. Llewellyn, F. Rouquerol, Stud. Surf. Sci. Catal. 160 (2007) 49–56.
[43] C.A. Emeis, J. Catal. 141 (1993) 347.
[44] V.P. Pakharukova, E.M. Moroz, D.A. Zyuzin, A.V. Ishchenko, L.Y. Dolgikh, E. Strizhak, J. Phys. Chem. C 119 (2015) 28828–28835.
[45] P.A. Sermon, K. Rollins, P.N. Reyes, S.A. Lawrence, M.A.M. Luengo, M.J. Davies, J. Chem. Soc. Faraday Trans. 1 (83(5)) (1987) 1347–1353.
[46] A.J. Marchi, J.L.G. Fierro, J. Santamaría, A. Monzón, Appl. Catal. A 142 (1996) 375–386.
[47] X. Xi, S. Ma, J.F. Chen, Y. Zhang, J. Environ. Chem. Eng. 2 (2014) 1011–1017.
[48] J. Gong, H. Yue, Y. Zhao, S. Zhao, L. Zhao, J. Lv, S. Wang, X. Ma, JACS 134 (34) (2012) 13922–13925.
[49] M. Berger, P. Fioux, S. Dorge, H. Nouali, D. Habermacher, E. Fiani, M. Vierling, M. Moliere, J.F. Brilhac, J. Patarin, Catal. Sci. Technol. 7 (18) (2017) 4115–4128.

[50] S. Li, Y. Tang, J. Zhang, W. Hao, W. Chen, F. Gu, Z. Hu, L. Li, Sep. Purif. Technol. 211 (2019) 684–696.

[51] J. Shan, H. Liu, K. Lu, S. Zhu, J. Li, J. Wang, W. Fan, J. Catal. 383 (2020) 13–23.

[52] R.-P. Ye, Y. Chen, T. Ramirez Reina, Z. Cao, T. Xu, X. Chen, Y. Jin, X. Li Zhang, J. Liu, Adv. Energy Sustain. Res. 2 (2021) 2100082.

[53] L. Xiaofei, Y. Ding Hua, C. Xuming, Petrochem. Technol. 39 (2010) 866–871.